A tidally driven estuary close to an amphidromy

Sissal Vágsheyg Erenbjerg[1,2], Jon Albretsen[3], Knud Simonsen[4], Erna Olsen[1], Eigil Kaas[2,5], and
Bogi Hansen[6]

[1]Dept. of Fjord Dynamics, Fiskaaling A/S, við Áir 11, FO-430 Hvalvík, Faroe Islands
[2]Niels Bohr Institute, Copenhagen University, Juliane Maries Vei 30, DK-2100 Copenhagen, Denmark
[3]Institute of Marine Research, P.O. box 1870 Nordnes, NO-5817, Bergen, Norway
[4]Dept. of Science and Technology, University of the Faroe Islands, J. C. Svabosgøta 14, FO-100 Tórshavn, Faroe Islands
[5]National Center for Climate Research, Danish Meteorological Institute, Lyngbyvej 100, DK-2100 Copenhagen, Denmark
[6]Faroe Marine Research Institute, P.O. 3051, FO-110 Tórshavn, Faroe Islands

Correspondence: Sissal Vágsheyg Erenbjerg (sissal@fiskaaling.fo)

Abstract. This paper describes the implementation of a high-resolution three-dimensional model of the estuary "Sundalagið Norður". This estuary is bound by narrow sills in both ends and has a large semidiurnal tidal variation. The proximity to an amphidromic region, results in a periodically varying difference in sea level height between both ends of the estuary, which generates strong semidiurnal tidal currents across the sills. The available observational data support the model results. The
5   model results verify the dominance of tidal forcing with semidiurnally varying volume fluxes into and out of the estuary. The amplitudes of these fluxes vary in strength with the fortnightly variation between spring and neap tides. More surprisingly, the model also indicates a strong fortnightly variation of net fluxes averaged over 25 hours reducing both diurnal and semidiurnal tidal currents. These variations are caused by fortnightly variations in sea level difference between both ends of the estuary, which are verified by comparison with observed sea level variations. This rather surprising result implies that exchanges within
10 the estuary and with its surroundings vary systematically; typically with one week of net northward flow followed by one week of net southward flow. This variation also appears to affect the mixing processes in the estuary and should be taken into account in planning development or activities. More observational data would be beneficial to validate the model more thoroughly and we recommend that a dedicated experiment with combined observations and numerical modeling is implemented.

1   Introduction

15 This study presents results from a high-resolution three-dimensional model of an estuary, "Sundalagið Norður", that is located in the Faroe Islands archipelago (hereafter: Faroes), in the North East Atlantic (Fig. 1a). The estuary is the northern part of a narrow sound separating the two largest islands in the archipelago and it is separated from the southern part of the sound by a narrow and shallow (4 meter deep) sill (the "Southern sill", Fig. 1b). In the northern end of the estuary there is also a sill (the "Northern sill", Fig. 1b), but it is wider and deeper (11 m) and leads to the open ocean on the Faroe shelf.

20   Throughout the sound, a number of villages release sewage and other effluents into the water that may affect the natural biota of the sound in various ways. The sound is also hosting two separate fish farming sites, one in the northern and one in the southern part. There is a potential for negative effects both on and from these sites, as well as interactions between the sites.
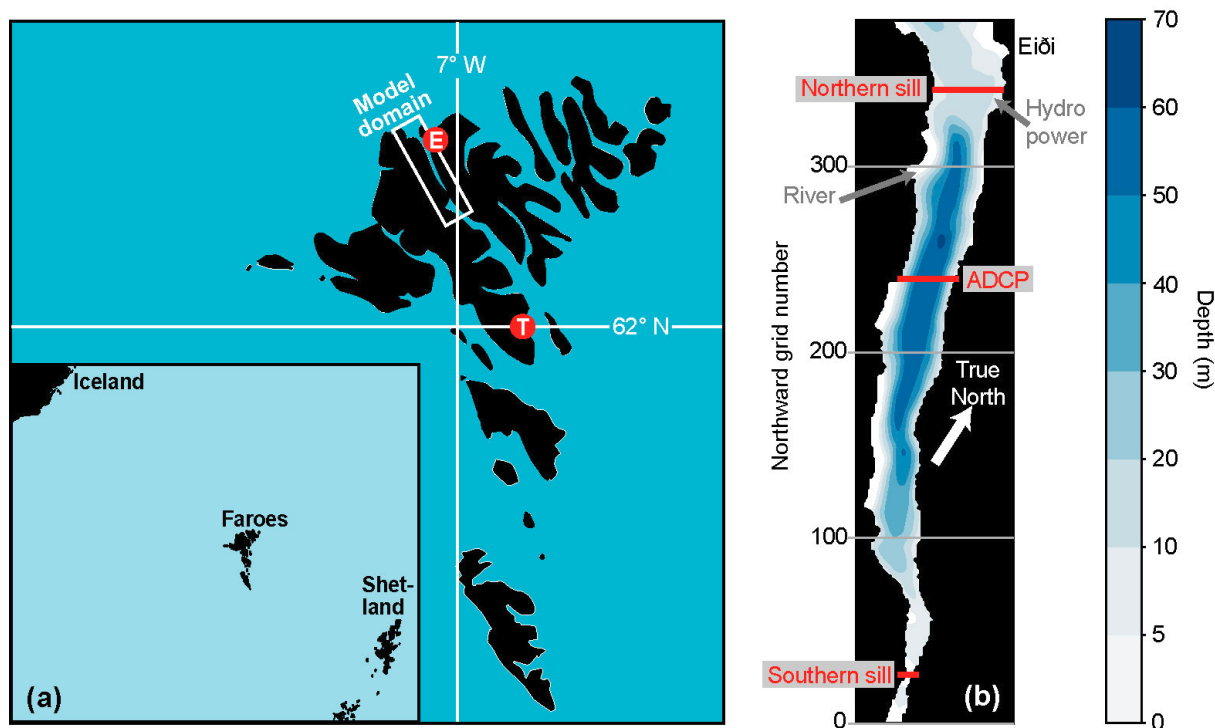
Figure 1. (a) The estuary studied in this paper is located within the white rectangle, which defines the model domain. The Faroes are situated between Iceland and Shetland (inset map). The red circles show two sites: Tórshavn (T) and Eiði (E) referred to in the text. **(b)** Bottom topography of the estuary. Freshwater supply from a river and a hydro-power plant are shown by grey arrows. Red lines indicate three cross-estuary sections discussed in the manuscript.

Thus, there is a need to understand the processes that mix and transport contaminated water between various parts of the sound and out of it.

25   This need has been augmented by the implementation of a hydropower plant with outflow into the northern part of the sound (Fig. 1b), reducing the runoff into the southern part of the sound while the northern part has received more freshwater. The outflow from the hydropower plant is by far the largest freshwater point source in the sound.

The classical terminology (e.g., Farmer and Freeland, 1983) describes a fjord as an estuary with a freshwater source at the head and a flow towards the mouth where a sill may be located. The estuary described in this paper is not a estaury in the

30   classical sense as it is open in both ends, however in many ways it behaves like a typical estuary.

The full model domain includes a wider area (Supplementary Fig. S1), but here, we focus only on the part of the domain that includes the estuary and areas just outside both ends (Fig. 1b). Although not running towards true North, we will in the following use the term "northward" (and southward) to describe the along-estuary variation as well as eastward (and westward) across the estuary.

35   The circulation in the estuary was investigated in the 1980s, which revealed that the bottom waters of the estuary would typically become stagnant during summer with reduced oxygen concentrations near the bottom as is common for Faroese sill fjords (Hansen, 1990). In this study, we focus, however, on the more "normal" conditions during winter, when the circulation is more similar to that of a non-sill estaury.

    The general theory for physical fjord oceanography from Farmer and Freeland (1983) states that the circulation in a estaury

40   is generally driven by freshwater (estuarine) forcing and wind stress at the surface. The freshwater entering the estaury has to flow out of it, but on its way, it entrains seawater and becomes a brackish out-flowing layer. To compensate, there must be an inflow of seawater. Since the brackish water is less dense than the seawater, the out-flowing brackish layer is typically on top of the in-flowing seawater layer although the Coriolis effect may influence this. On long time scales, this "estuarine circulation" will typically dominate, but strong wind stress may disrupt it.

45   In the present case, these two forcing mechanisms are joined by a third: tidal forcing, which is complicated by the fact that the southern part of the sound is close to an amphidromic region for the semidiurnal tides. An amphidromic region is characterized by a small tidal amplitude while the cophase lines have strong horizontal variations. Thus, the amplitude of the M_2 tide is much smaller south of the sound than due north of it (Simonsen and Niclasen, 2021). This induces a strong periodically varying barotropic pressure gradient through the estuary.

50   To understand how these various forcing mechanisms affect mixing and circulation within and out of the estuary, a numerical model is essential. Previous modeling efforts have mainly been based on barotropic two-dimensional models (Simonsen and Niclasen, 2021; Kragesteen et al., 2018). However Rasmussen et al. (2014) and Erenbjerg et al. (2020) have also reported results from full three-dimensional models of the Faroe shelf, but both those models were too coarse to resolve the conditions within the estuary. To resolve the processes within our estuary, a high resolution, three-dimensional ocean model is imperative

55   and such a model will also be necessary to investigate the connectivity between the Faroese fish farming sites in the future.

    We have therefore implemented such a high-resolution model (32m x 32m horizontal, 35 vertical layers) that is one-way triply-nested within a 4 km × 4km ROMS model (Fig. Supplementary S1), which covers the area from the North Atlantic west of Ireland, the Nordic Seas and into the Arctic to the north (Lien et al., 2013). The high-resolution model was run for 29 days in January-February 2013 with realistic atmospheric forcing. This model should have a sufficiently high resolution to simulate

60   Faroese estuaries and sounds. It also appears to be a powerful tool for planning and managing fish farming and investigating the effects of hydropower development or other anthropogenic interventions affecting the waters.

    Prior to practical model applications, the model must be validated and one reason for choosing this particular estuary is that it has been the object of a large observational effort. This includes measurements of current velocity during the modeling period as well as hydrographic properties (temperature and salinity) over several years. One aim of this study was therefore to

65   validate the model against these observations. At the same time, the model output has delivered new information on mixing and transport processes in the estuary, which may be of more general interest.

Ocean Science
Discussions

Open Access

2 Material and methods

2.1 The model

In this paper we have applied a model setup based on the open-source Regional Ocean Model System (ROMS, http://myroms.org,
70 Shchepetkin and McWilliams, 2005; Haidvogel et al., 2008). This is a state-of-the-art three-dimensional hydrostatic, free-
surface, primitive equation solving ocean model. ROMS applies generalized terrain following s-coordinates in the vertical and
regular horizontal grids. This setup applies 32 m × 32 m resolution in the horizontal and 35 vertical layers. The triply-nested
setup (Supplementary Fig. S1) is forced along the four open boundaries by SVIM (4 km × 4 km horizontal resolution Lien
et al. (2013)), the first nesting has a resolution of 800 m in the horizontal and is further described in Erenbjerg et al. (2020).
75 The second nesting contains a 160 m horizontally resolved grid and is run for five months in 2013. This second nesting is used
as forcing for the ultra-high-resolution setup used in our current study.

Atmospheric forcing is provided by the Weather Research and Forecasting (WRF) model on the surface. The WRF-model is
set up with a configuration that has a resolution of 9-3-1 km in the horizontal and the area with 1 km × 1 km resolution covers
the entire Faroe Islands. More detail on configuration can be found in Myksvoll et al. (2012).
80 The freshwater input to the estuary from runoff is assumed to be constant in time and based on two reports: Erenbjerg (2020)
and Davidsen et al. (1994) as well as data from the local energy supplier. The two freshwater sources are a hydropower plant
on the eastern coast and a river on the western coast (Fig. 1b). Their average annual supplies are 1.7×10^8 m^3 and 6.3×10^7
m^3, respectively. The entire annual freshwater input from runoff is averaged and divided into a constant daily input to ROMS.

The computationally demanding model was run from the 11th of February until the 12th of March 2013. To avoid potential
85 spin-up effects, results from the first day have been omitted. Model output was stored every hour and includes horizontal
velocities, temperature, and salinity for each grid cell (Arakawa C grid). Sea level height was also stored for each surface grid
cell.

2.2 Observations

During the modeling period, two upward-looking Acoustic Doppler Current Profilers (ADCPs) were deployed on the bottom
90 of the estuary (Fig. 1b). Details are documented in Larsen et al. (2014a, b). From 2012 to 2018 there were a high number
of CTD (Conductivity Temperature Depth) observations in the estuary, most of them documented in Simonsen et al. (2018)).
Unfortunately, no hydrographic observations were made during the modeling period. Sea level measurements are available at
two sites "Eiði" and "Tórshavn" (Fig. 1a) from the Faroese Office of Public Works (Landsverk). These measurements have
many gaps, but they are sampled every ten minutes, which allows generation of the hourly averages that are used here.

3 Model validation

3.1 Current velocity validation

The two ADCPs were located on a transect crossing the estuary (Fig. 2a), but quality data were only obtained for the deep parts of the velocity profiles (Larsen et al., 2014a, b). Modelled and observed average cross-estuary profiles are similar and close to zero (Fig. 2b and 2c). For mooring site BW (Fig. 2b), the modelled and observed along-estuary profiles are also fairly similar for the depths reached by the ADCP. For mooring site BE (Fig. 2c), the discrepancy is larger, but Fig. 2a indicates that this site is close to a transition zone between northward and southward flow at depth, which makes the comparison sensitive to modeling details.

Instantaneous velocities in the estuary will depend highly on the phase of the tidal signal. In the model, this is determined by the forcing along the outer boundaries. Thus, a model-observation comparison of instantaneous velocities is not very meaningful. Instead, the top panels in Fig. 3 compare observed and simulated along-estuary velocities averaged over consecutive 25-hour periods (to average out the tides). The observed and simulated velocities are certainly not identical, but they are generally of the same magnitudes. All of the correlation coefficients are also positive and three out of four are significantly higher than zero at the 95 % level ($p < 0.05$).

On daily time scales, the model is able to reproduce velocity variations to a significant extent. A similar conclusion can be reached for shorter time scales including the tidal velocity variations, which is documented in the bottom panels of Fig. 3. For both the top and the bottom panels, the largest discrepancy between observations and model is for 18 m depth at mooring site BW. From Fig. 2a it appears that this is close to the average interface between northward flow in the upper layers and southward flow at depth. Thus, details of model topography, setup, and forcing may affect the comparison for this case disproportionally.

3.2 Salinity validation

As for other estuaries, a key feature of our estuary is the interplay (mixing, transport) between the freshwater added from land or the atmosphere and the saline seawater entering the estuary over the two sills. This interplay is especially reflected in the salinity distribution. To assess the model performance for this parameter, we collected the data from all the CTD observations in the estuary 2012 – 2018 (details are documented in Simonsen et al. (2018)).

In the shallow regions on either side of the estuary, detailed bottom topography and proximity to a river outlet may affect the salinity disproportionately. We therefore considered only CTD casts with bottom depth at least 50 m. To exclude situations with a stagnant bottom layer, we only used observations from winter (November – April). This gave a total of 92 salinity profiles, which are shown as the thin black lines in Fig. 4.

The semi-transparent red area in Fig. 4 shows the range of daily averaged salinity profiles from model grid cells that fulfill the same criterion for bottom depth. One clear difference is that the observed salinities are lower than the range from the model even at depth. This is not surprising since the salinity of the shelf water decreased considerably from 2013 to 2018 (Erenbjerg et al., 2020).
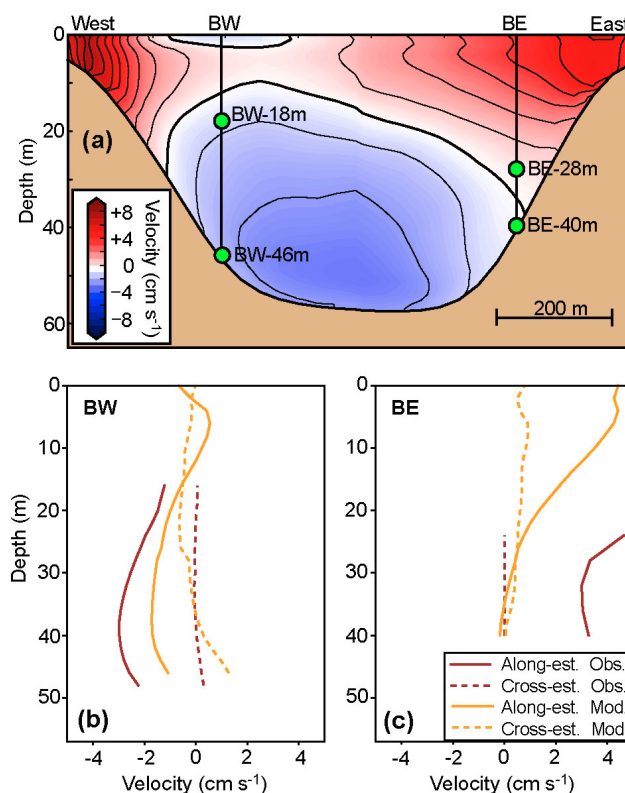
Figure 2. (a) Distributions of northward velocity along transect labeled "ADCP" in Fig. 1b averaged over the simulation period. The two vertical lines labeled "BW" and "BE" indicate the locations of two ADCPs moored on the bottom and green circles indicate the uppermost and lowermost depths with high-quality measurement for each of the ADCPs. **(b)** and **(c)** Velocity profiles along the estuary (continuous curves) and across it (dashed curves) from the ADCP measurements (dark curves) and the model (light curves) at the two mooring sites averaged over the modeling period.

The decreasing salinity cannot explain the large differences in the upper layers where the observations show that the water often was much fresher than indicated by the model. Still keeping in mind, that the two data sets have different conditions. The model was run over one month with nearly constant freshwater supply, whereas the observations are over a six-year period with variable precipitation, river runoff, hydropower outflow.

4   Model results

There are no indications of serious spin-up effects, but for precautionary reasons we omit the first day of the simulations. Thus, the model output comprises 672 hourly values (from 12 February 01:00 to 12 March 00:00) of velocity and hydrographic parameters for each grid cell as well as sea level. This period will in the following be referred to as the ***"simulation period"***. We define our ***"estuary"*** to be the region between the two sills. The sills are defined by minimum cross-sectional (east-west)
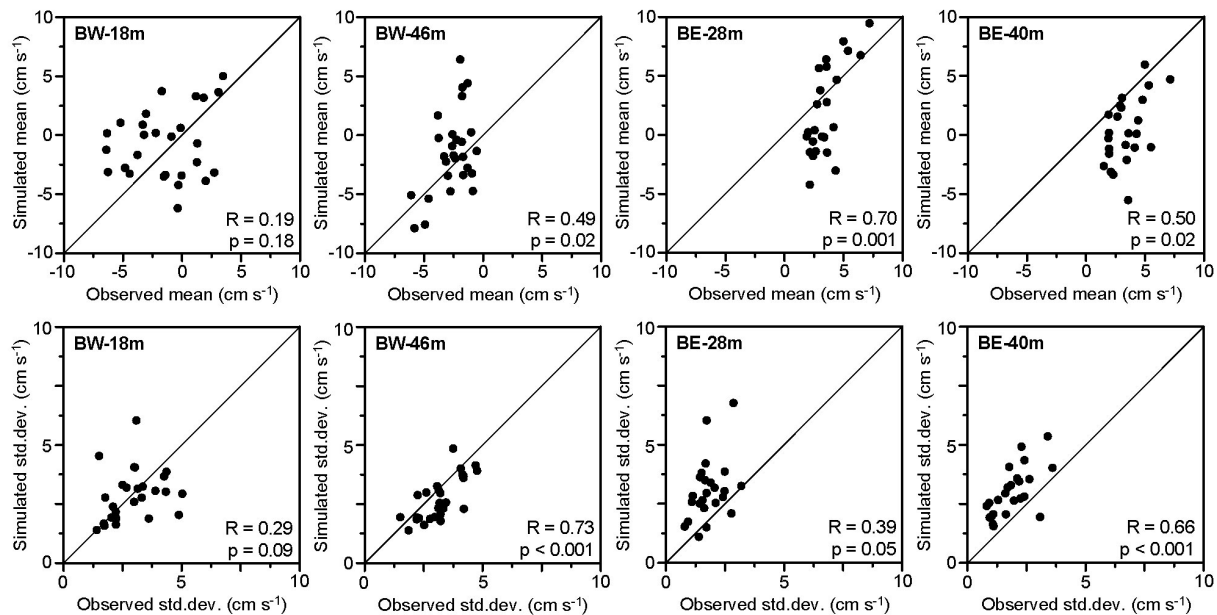
Figure 3. Comparison between observation and model for averages (top panels) and standard deviations (bottom panels) of along-estuary velocity for consecutive 25-hour periods at two measurement depths for each of the ADCP sites (Fig. 2a). Correlation coefficients (R) and their statistical significances (p) are listed in the lower right corner of each plot. The statistical significance has been corrected for serial correlation by the "modified Chelton" method recommended by Pyper and Peterman (1998). Diagonal lines indicate equality between model and observation.

area and located at the red lines in Fig. 1b. The total volume between the sills is 2.31×10^8 m³ with a surface area of 8.75 $\times 10^6$ m². Average distributions of hydrographic properties and velocity for the whole simulation period (Supplementary Fig. S3) give an indication of the estuarine characteristics, but may be rather misleading due to the large and systematic changes through the period.

4.1 Hourly variations

On hourly time scales, the flow through the estuary is clearly dominated by the tides. This is evident in Fig. 5a, which shows the hourly variations of volume fluxes across both the northern, $q_N(t)$, and the southern, $q_S(t)$, sill, during the 4-week simulation in 2013, where positive values indicate northward volume flux and negative values indicate southward flux. The semidiurnal variation is clear in the hourly output, as is a fortnightly variation in the amplitude of the flux. The amplitude of the flux across the northern sill is much higher than the amplitude in flux across the southern sill. From a regression analysis, the highest correlations are found when $q_S(t)$ lags one hour after $q_N(t)$, and the amplitude ratio is then 0.46 (Table 1).

Typically, the volume flux is in one direction for six hours before changing sign. Adding up all the water flowing into or out of the estuary across the northern sill during one of these tidal phases, we find that this typically is around 10 % of the
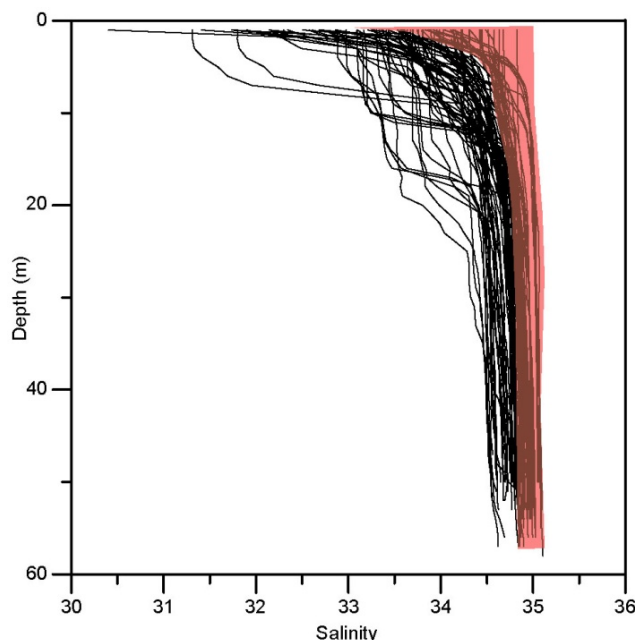
Figure 4. Comparison of salinity profiles from observations and model. The black lines show observed salinity profiles from 92 individual CTD casts at stations with bottom depth at least 50 m in winter (November – April). The semi-transparent red area in front is the salinity range (minimum to maximum at each depth) of daily averaged salinity profiles for all grid cells in the model with a bottom depth of at least 50 m.

volume, but occasionally the phases may last longer and transport more water, such as the period by the end of the first week
150   of simulation where an episode of excess southwards flow flushes 30 % of the volume out (Fig. 5b).

Sea-level variations also follow the tidal cycle. We have defined four hourly sea level time series: $h_N(t)$ is sea level north of the northern sill. $h_S(t)$ is sea level south of the southern sill. $h_{IS}(t)$ is sea level just north of the southern sill. $h_I(t)$ is sea level averaged over all surface grid points between the two sills. In addition, $\Delta h_S(t)$ is the sea level difference across the southern sill, $h_{IS}(t) - h_S(t)$ (Supplementary Fig. S4).

155   Correlation coefficients (R) between some of these parameters are listed in Table 1. Average sea level between the two sills, $h_I(t)$, is very highly correlated with sea level north of $h_N(t)$, with zero lag (less than one hour) and a regression coefficient (α) close to one. Even $h_{IS}(t)$, just north of the southern sill (Supplementary Fig. S4), follows $h_N(t)$ almost identically. Thus, sea level within the estuary responds more or less instantaneously to the sea level north of the estuary. Sea level south of the estuary, $h_S(t)$, is also highly correlated with $h_N(t)$, but with a smaller regression coefficient (Table 1).

160   Hourly values for volume flux across the two sills are fairly well correlated with the difference in sea level between both ends of the estuary, $h_N(t) - h_S(t)$, consistent with the idea that this difference drives the flow through the estuary. The volume flux across the southern sill, $q_S(t)$, is better correlated (R=-0.95) with the sea level change across the southern sill, $\Delta h_S(t)$ (Supplementary Fig. S4), but an even better fit is obtained by a quadratic fit, rather than a linear one (red curve in Fig. 6).
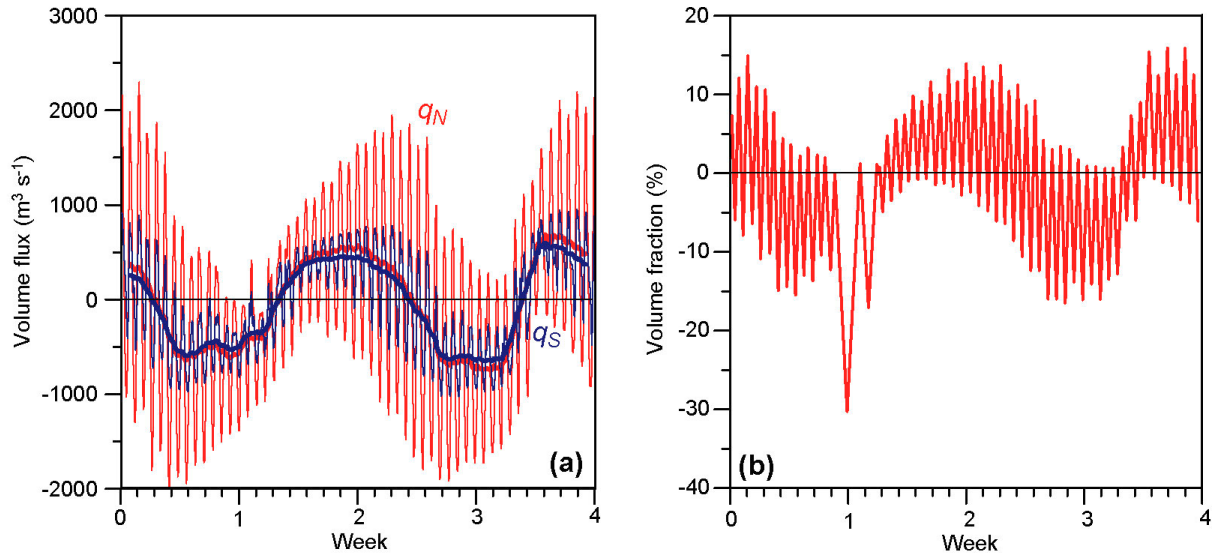
Ocean Science
Discussions

Figure 5. (a) Hourly (thin lines) and 25-hour averaged (thick lines) northward volume transport across the northern sill, q_N, (red) and across the southern sill, q_S, (blue). **(b)** Fraction of total volume transported into (positive) or out of (negative) the estuary across the northern sill during each uni-directional period.

Table 1. Lagged correlation and regression analysis of relationships between hourly values of various model parameters. R_0 is the correlation coefficient for zero lag. Lag_{max} is the lag (in hours) that gives the numerically highest correlation coefficient. R_{max}, α_{max}, and β_{max} are the correlation coefficient and the regression coefficients for that lag.

Regression equation	R_0	Lag_{max}	R_{max}	α_{max}	β_{max}
$q_S(t+lag) = \alpha \cdot q_N(t) + \beta$:	0.84	1	0.87	0.46	-36 $m^3 s^{-1}$
$h_I(t+lag) = \alpha \cdot h_N(t) + \beta$:	>0.99	0	>0.99	1.01	0.04 m
$h_{IS}(t+lag) = \alpha \cdot h_N(t) + \beta$:	>0.99	0	>0.99	1.01	0.01 m
$h_S(t+lag) = \alpha \cdot h_N(t) + \beta$:	0.96	0	0.96	0.89	-0.05 m
$q_N(t+lag) = \alpha \cdot [h_N(t) - h_S(t)] + \beta$:	-0.88	0	-0.88	-7606 $m^2 s^{-1}$	346 $m^3 s^{-1}$
$q_S(t+lag) = \alpha \cdot [h_N(t) - h_S(t)] + \beta$:	-0.94	0	-0.94	-4349 $m^2 s^{-1}$	165 $m^3 s^{-1}$
$q_S(t+lag) = \alpha \cdot \Delta h_S(t) + \beta$:	-0.95	0	-0.95	-4367 $m^2 s^{-1}$	228 $m^3 s^{-1}$

The quadratic fit (red equation in top right corner of Fig. 6) is motivated by a simple model for the flow across the southern
165 sill, in which the speed at any instant, $v_S(t)$, is assumed to be homogeneous on the section. If friction is ignored, the Bernoulli equation links the kinetic energy of the flow (proportional to speed squared) to the loss in potential energy (proportional to $\Delta h_S(t)$). The volume flux is given as $q_S(t) = A \cdot v_S(t)$, where A is the cross-sectional area over the sill in the model (= 670 m^2). This leads to the red equation in the top right corner of the figure where the parameter δ is to adjust for the fact that the
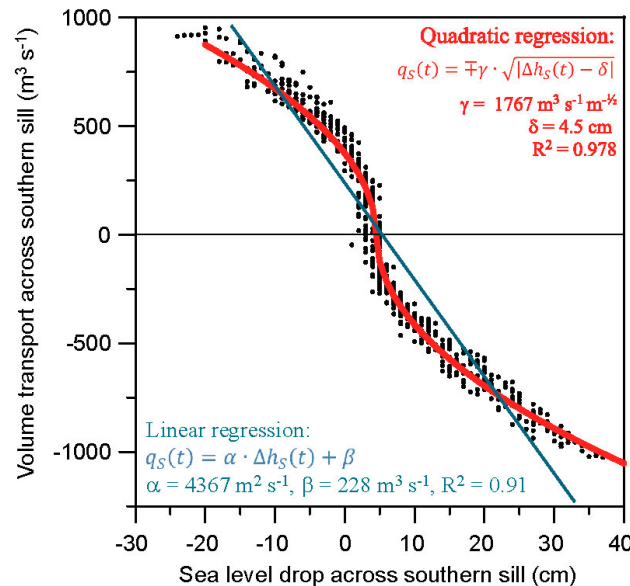
Figure 6. Volume transport across the southern sill, $q_S(t)$, plotted against sea level change across the southern sill, $\Delta h_S(t)$, both from the model (Supplementary Fig. S4). Each dot represents one hour. The blue line represents the linear regression line from Table 1 with coefficients shown in the lower left corner. The red curve represents the result of a least squares fit to the red equation shown in the upper right corner (quadratic regression). The $\pm$ symbol in the equation indicates that $q_S(t)$ has the opposite sign of $\Delta h_S(t)$-δ. The linear fit (blue line and equation) explains 91 % of the variance of $q_S(t)$. The quadratic fit (red curve and equation) explains 97.8 %.

locations for sampling $\Delta h_S(t)$ (Supplementary Fig. S4) were chosen arbitrarily. The value for γ was derived by fitting the
170   model data into this simple framework. When friction is included, the speed and volume transport decrease and the value for γ
in the fit changes (Fig. 6) this indicates that a considerable part of the potential energy is lost to friction .

4.2   Fortnightly variations

The fortnightly variation of tidal flux amplitude seen in Fig. 5a is a normal phenomenon in Faroese waters (Hansen, 1978),
reflecting the variation between neap and spring tides. However, the fortnightly variations in the 25-hour average fluxes (thick
175   lines in Fig. 5a) are unexpected. The simulation period includes two full periods with net southward flow and one period with
net northward flow, all of them lasting about one week (Fig. 7a). Both the first days and the last days during the simulation
have a net northward flow. This figure also has a curve (black) that shows the variation of the standard deviation of $q_N(t)$
over consecutive 25-hour intervals. This curve should reflect the strength of the tidal amplitude and it is worth noting that the
25-hour average flux does not reach its extremes during spring tide, but rather a few days out of phase (Fig. 7a).
180   To help understand the fortnightly flux variations, Figure 7b shows 25-hour averages and standard deviations of sea level
height. During the periods with average southward flux, average sea level is higher north of the estuary. When the average flux
is northward, the average sea level is higher south of the estuary. Consistent with Table 1, the volume flux through the estuary
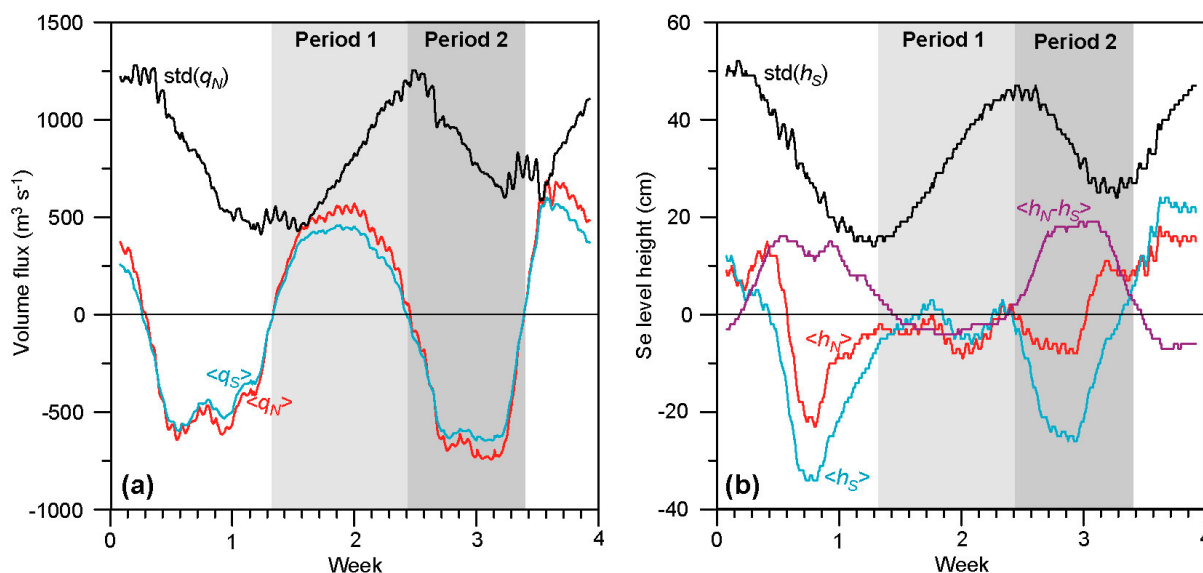
Figure 7. Daily (25-hour) averages (<>) and standard deviations (std) within each 25-hour period for **(a)** volume transports and **(b)** sea level heights. The standard deviations ought to be dominated by the strength of the tidal amplitudes and should therefore reflect the variation between spring and neap tides. The shaded areas indicate two periods discussed in the text: "Period 1" lasting 188 hours from 21 February 08:00 to 1 March 03:00 and "Period 2" lasting 158 hours from 1 March 04:00 to 7 March 17:00.

may be seen as forced by the sea level difference between both ends. In this paradigm, the reason for the fortnightly variations in volume flux is the variation in this sea level difference.

185   Figure 8 shows the selected two full periods of northward and southward flow, respectively. Period 1 is the first full period with average northward flow, whereas Period 2 is the following period with average southward flow. To illustrate the differences between these two periods, northward velocity and salinity are averaged over each period and across (east-west) the estuary and then plotted against northward grid number and depth in Fig. 8.

During period 1 (upper panels in Fig. 8), the average flow is northwards through the upper parts of the estuary, down to 190   20-30 m depth except for the water over the northern sill. This indicates that during this period the upper parts of the estuary are refilled by the water entering from the south. In the bottom part of the estuary, Period 1 has average southward flow. Across the northern sill a thin layer of seawater is entering the sill with a velocity of up to $2 \, \mathrm{cm \, s^{-1}}$ on average. This water immediately flows towards the bottom of the basin where it is mixed into the water column partially and transported southwards.

From the average salinity during period 1 (upper panels in Fig. 8), it seems that the entering seawater is highly diluted on 195   the way into the basin. Only a very small part of the entering seawater in Period 1 is undiluted once reaching the bottom of the basin. For the upper most layers in the basin the salinity is low, and it appears that freshwater is added from the south.

During Period 2 (lower panels in Fig. 8), the average velocity is southwards throughout most of the estuary. This implies, that the southern part of the sound receives a net inflow of water from our estuary. Except for some minor areas close to the
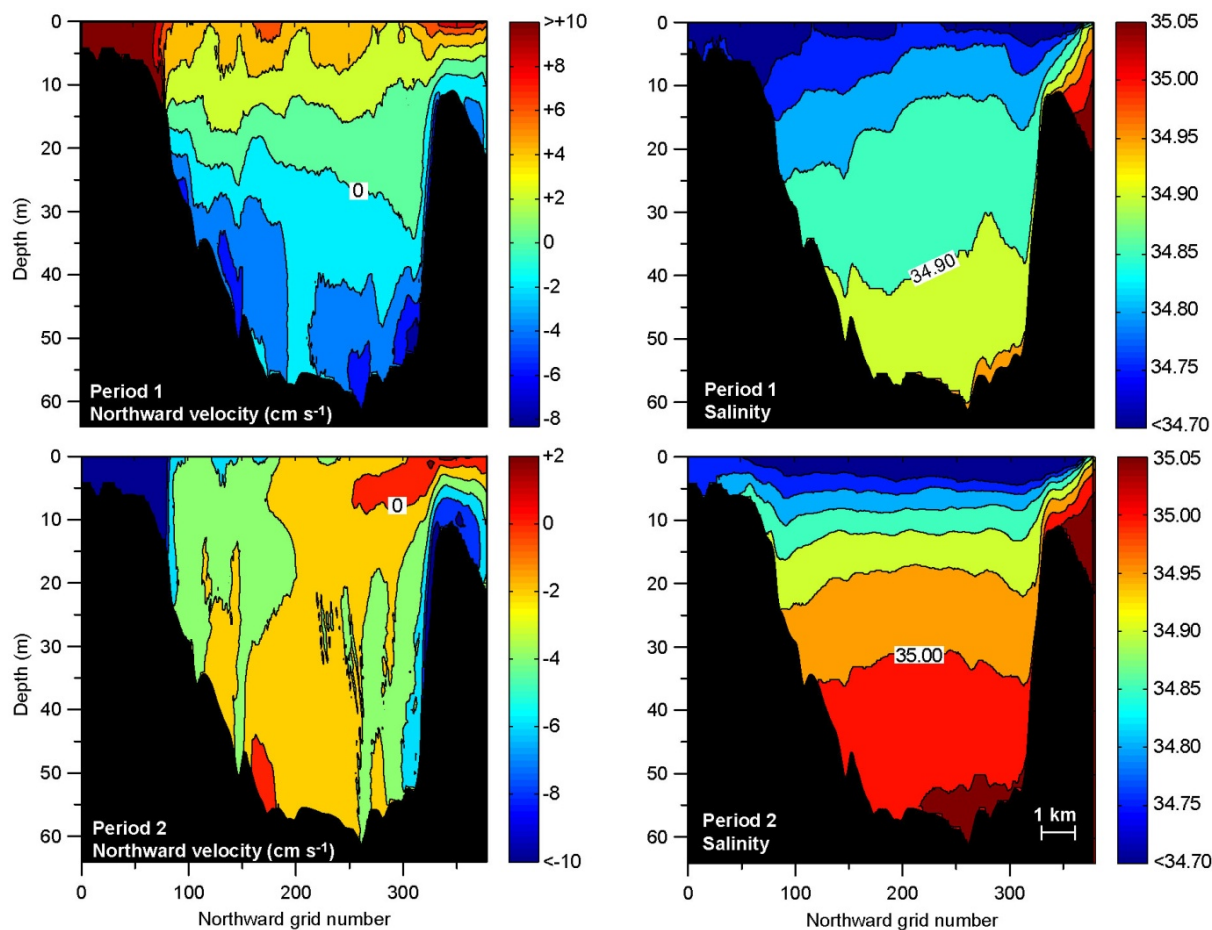
Ocean Science
Discussions

Figure 8. Cross-estuary averaged northward velocity and salinity plotted against northward grid number for the two different periods defined in Fig. 7. For velocity, the highest (top left panel) or lowest (bottom left panel) values are grouped together. Note different velocity scales. For salinity, the lowest values are grouped together. The bottom depth indicated by the black areas is the maximum depth along each section crossing the estuary.

bottom, the only northward flow during Period 2 is near the surface over and just south of the northern sill. This appears to be

200   freshwater from the river and hydropower plant in the northern part of the estuary (Fig. 1b).

The average salinity distribution during Period 2 (lower panels in Fig. 8), indicates that seawater enters the estuary over the northern sill and fills it up from below. Thus, almost undiluted seawater fills the basin below 30 m depth. Almost no freshwater seems to be mixed below 20 meters depth during this period in contrast to Period 1 where a large amount of the freshwater is mixed into the water column.
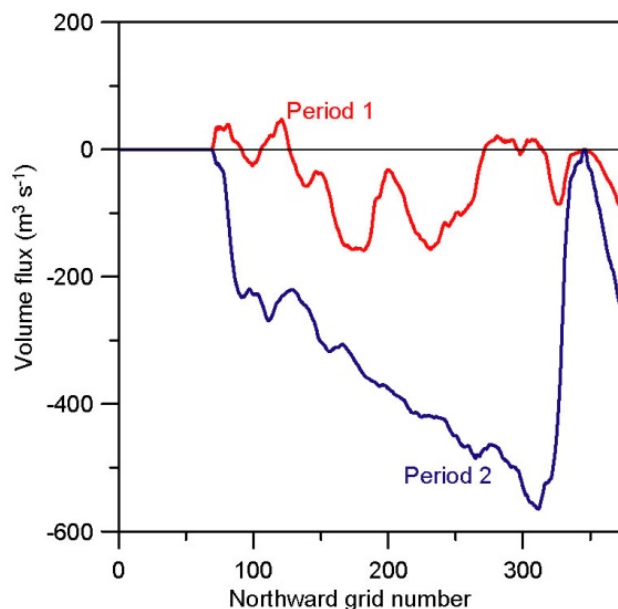
Figure 9. Northward volume flux through (east-west) cross-sections below sill depth of the northern sill (from 12 m, downwards) for the two different periods indicated in Fig. 7.

205   The difference between the deep flow during the two periods is illustrated in the period-wise averages in Fig. 9, showing volume flux below sill depth of the northern sill (11 m). From this figure it is clear that the volume flux through the deep parts of the estuary is much greater during Period 2.

4.3   Observational validation of fortnightly variations

The fortnightly variations in average fluxes and sea level differences (Fig. 7) were, as mentioned, unexpected. To check that
210   these variations are not purely an artifact generated by the model, we have compared observed sea level at "Eiði", which is just north of the estuary with the observed sea level in Tórshavn, which is south of it. When averaged over 25 hours, the sea level at both sites is dominated by atmospheric pressure variations (Supplementary Fig. S5). This effect is strongly reduced when the average difference in sea level between both sites is considered, which instead varies consistently with the neap-spring variation of the amplitude of the semidiurnal and diurnal tide (Fig. 10).

215   For zero lag, the daily (25-hour) averaged sea level difference between the two sites is positively correlated with the tidal amplitude of sea level variations in Eiði with a correlation coefficient $R = 0.50$, which is significantly different from zero at the 98 % ($p < 0.02$) level. The correlation increases slightly for a lag of 1 day (Fig. 10a), which implies that the 25-hour average sea level difference (north minus south) is highest shortly after spring tides. This is consistent with Fig. 7b, although the lag there seems somewhat larger. Remarkably, the (numerically) highest correlation, $R = -0.55$, is found when the sea level difference
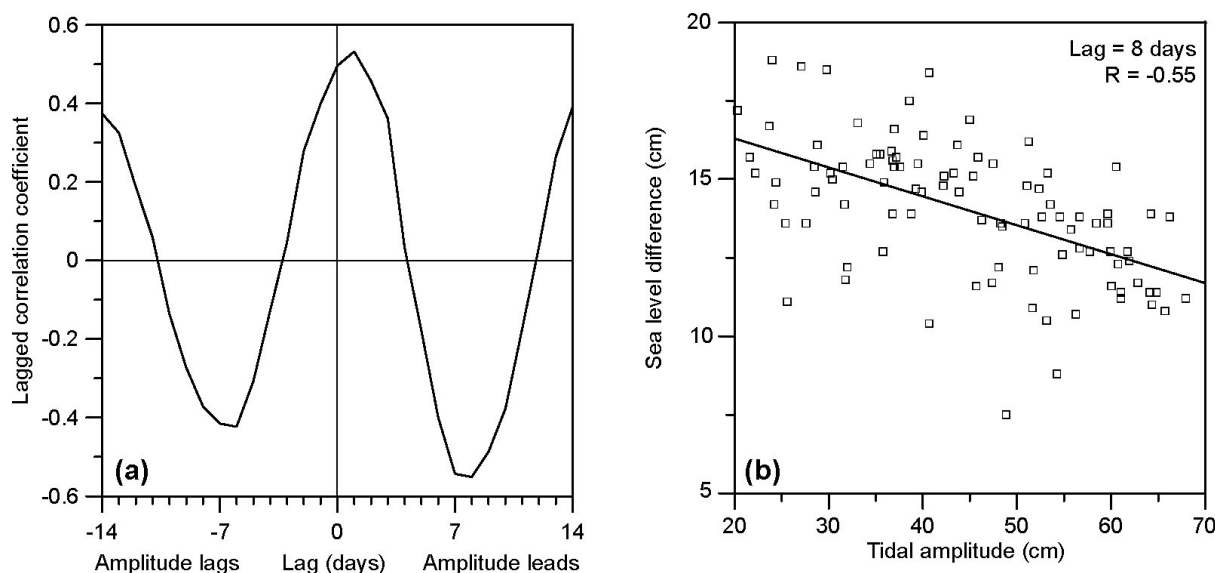
Figure 10. Comparison of daily (25-hour) difference in observed sea level between Eiði and Tórshavn (Eiði minus Tórshavn) and the tidal amplitude in Eiði defined as the standard deviation of sea level for each 25-hour interval based on observed sea level for the first four months of 2013. **(a)** Lagged correlation coefficient between the two parameters. **(b)** Sea level difference plotted against tidal amplitude in Eiði for a lag of 8 days with the regression line shown.

220   lags after the tidal amplitude by 8 days (Fig. 10a), i.e., shortly after neap tide. This supports our conclusion that the observed fortnightly sea level variations are real and not an artifact of the averaging.

4.4   Density inversions downstream from the northern sill

From the salinity distributions in Fig. 8 right, it seems that the seawater entering the estuary across the northern sill is flowing downwards and is then mixed with the water inside the estuary just downstream of the sill. To study this in more detail, the
225   density structure was plotted along a track (Fig. 11a). The track was chosen based on the average maximum velocity close to the bottom, beginning on the shallow part of the sill (track number 0) down-slope to 55 m depth (track number 35). The average velocity during the entire simulation period is more than 10 cm s^{-1} southwards in the bottom layer of the steep slope of the track (Fig. 11d).

As long as turbulent mixing is weak, the density structure is normally stable with density increasing downwards. Density
230   inversions with density decreasing downwards may therefore be used as a sign of mixing. To utilize this, we define a *"density inversion"* as the density difference between the third lowest layer and the bottom layer (upper minus deeper) when this value is positive the density is inversed. Under stable conditions, when this value is negative, it is set to zero. The spatial and temporal variations of density inversions along the selected track are illustrated on the Hovmøller diagram (Fig. 11b).
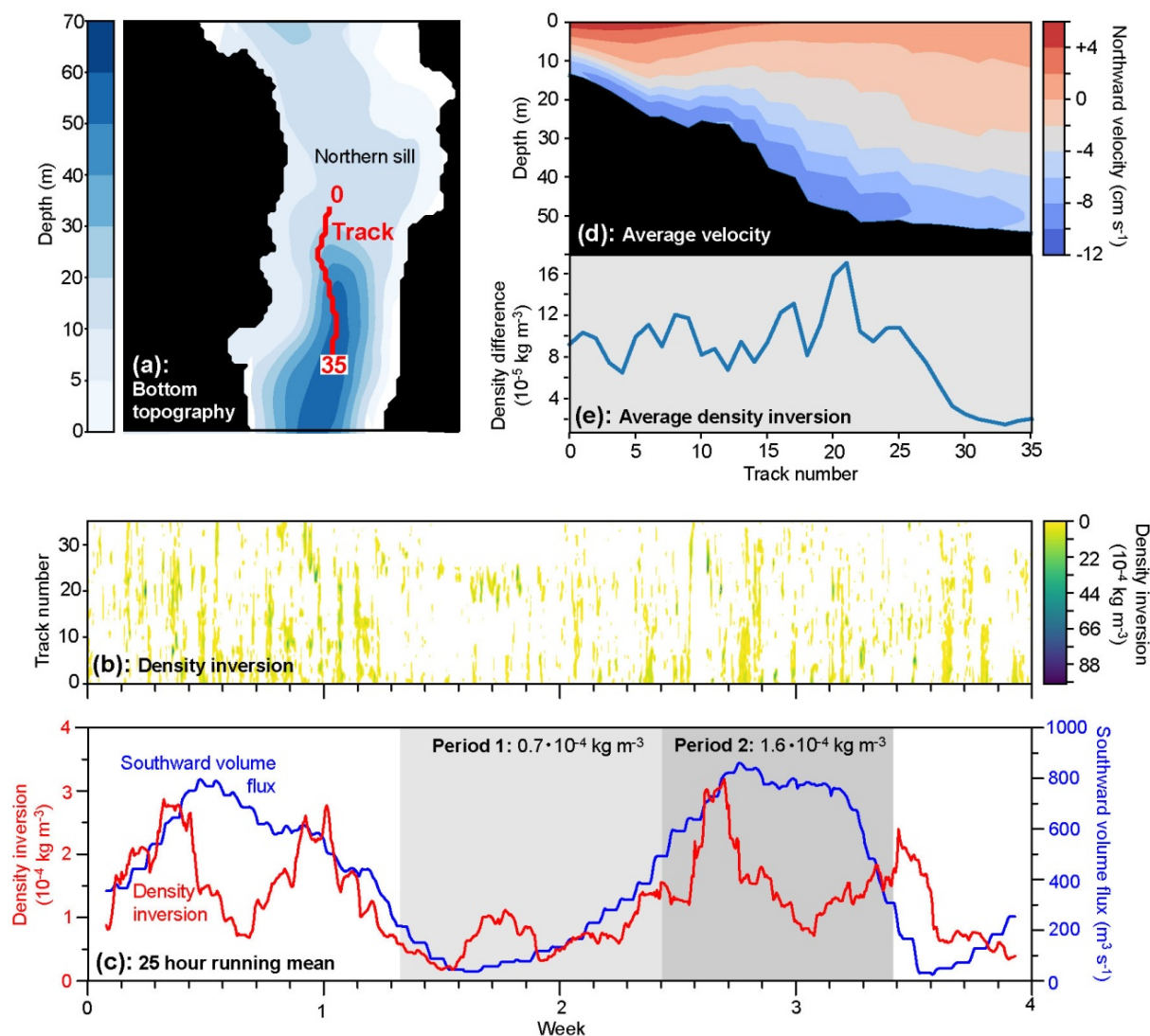
Ocean Science
Discussions

Open Access

Figure 11. (a) Bottom topography around the northern sill. The red line shows a track with numbers ranging from 0 to 35, which are used in the other panels. (b) Density inversion, defined as density (σ_Θ) difference between the deepest layer and two layers above (layer 2 minus layer 0) along the track every hour. Only positive values are shown (negative values white). (c) The red curve shows the density inversion in the panel just above averaged over all track numbers and 25-hour running mean. The blue curve is 25-hour running mean of southward-directed volume flux (positive towards the south) across the northern sill (set to zero for hours with northward flux). The shaded areas indicate the two periods defined in Fig. 7 with average density inversion for each period shown. (d) Average northward velocity at various depths along the track. (e) Density inversion along the track averaged over the whole period.

If the density inversions are averaged over the track and temporally smoothed, they exhibit systematic variations (red curve in Fig. 11c). Most pronounced is the rather frequent occurrence of inversions in the first part of the simulation from day two

to nine. From day nine to 15, the density inversions are less frequent for most part of the track except for track points 20-25. These variations show some similarity to the variations in Fig. 7a and verified by the blue curve in Fig. 11c. Strong southward flow across the northern sill seems to be a necessary – but not sufficient – condition for density inversion.

When averaged over time, the density inversions mainly occur on the down-hill slope, and are maximal right before the bot-
240 tom slope levels off at track number 20, Fig. 11e. This could indicate hydraulic jump conditions, although we use a hydrostatic model and cannot conclude on any vertical advection.

5 Discussion

5.1 Model performance

The comparison between average velocities in the model and in observations (Sect. 3), did not show identical values, but taking
245 into account the spatial variation (Fig. 2a) the corrrespondence is as good as may be expected. For temporal velocity variations, most of the corrrelations between model and observations (Fig. 3) were significant at the 95 % (p <0.05) level, which again is encouraging. No hydrographic observations were made in the estuary during the simulation period.

5.2 Hourly variations

On short time scales, the flow through the estuary is clearly of tidal character with semidiurnal dominance (Fig. 5a) and we
250 expect sea level differences between both ends to be the main driving force. This is supported by the high corrrelations between volume fluxes across the sills, $q_N(t)$ and $q_S(t)$, and sea level difference $h_N(t) - h_S(t)$ (Table 1).

As the tidal wave enters the estuary from the north, it should propagate southwards as a barotropic wave with sufficient speed to pass through the estuary in less than an hour. This is verified by the high zero-lag corrrelations between $h_N(t)$, $h_I(t)$, and $h_{IS}(t)$ (Table 1). Most of the sea level change occurs over a fairly short distance over the southern sill and this is where
255 the highest speeds are observed (Supplementary Fig. S6).

Speeds exceeding 2.5 m s^{-1} might seem excessive, but according to local sailors, the speeds over the southern sill may occasionally be considerably higher. From the arguments supporting the quadratic fit in Fig. 6, it appears that a considerable part of the potential energy in the sea level is lost to friction over the southern sill. Thus, the flow across the southern sill probably controls how much water the tides can push through the estuary, but this will also make the results sensitive to
260 turbulence and bottom friction parameterization in the model.

To reach the high values for speed (Supplementary Fig. S6) and volume transport (Fig. 5a), strong forcing is required. This forcing is achieved through the periodically varying large differences in sea level between both ends of the estuary and they may be linked to the amphidromic character of the region. The "textbook" amphidromy is a point in the middle of an ocean basin, around which the tidal wave turns. Here, the islands complicate matters, but Hansen (1978) suggested that an
265 amphidromic region for the semidiurnal tides was located somewhere in the proximity of Tórshavn based on tidal analysis of sea level observations there. Combining sea level observations and modelling, this has been more thoroughly investigated by

Simonsen (1992) and Simonsen and Niclasen (2021). Their tidal chart for the M_2 constituent has a semi-amphidromic point a short distance east of Tórshavn and their amplitude of M_2 sea level is much higher (60 cm) north of our estuary than south of it (10 cm).

270   From these results, we might expect sea level differences between both ends of the estuary to exceed 50 cm at times. In the model, they are smaller than that (Table 1 and Fig. 6), which may well be because our location for sea level south of the estuary, $h_S(t)$, is still close to the southern end of the estuary and probably affected by the sea level inside. Nevertheless, the sea level differences in the model are sufficient to generate the potential energy needed to accelerate the flow across the controlling section over the southern sill even though it is slowed down by friction (Fig. 6).

275   **5.3   Fortnightly variations**

As demonstrated in Fig. 5 and Fig. 7, fortnightly variations are seen; not only in the tidal amplitude, but also in 25-hour averaged volume flux. Is this an artifact of the processing? On the Faroe shelf, the tides are dominated by semidiurnal and diurnal variations that vary in amplitude fortnightly, mainly as an interference between the M_2 tide (period 12.42 hours) and the S_2 tide (period 12 hours). For these variations, a 25-hour mean will average out close to zero. There will be a residual, but 280   it should not exceed the maximum tidal amplitude divided by 25. We expect this residual to vary fortnightly in phase with the strength of the tidal amplitude.

The simulated variations in 25-hour averaged volume flux are much larger than this expected residual. At times, the 25-hour averaged flux equals the standard deviation of the flux during the same 25 hours and the average flux is not in phase with the amplitude (Fig. 7a). Thus, we conclude that these fortnightly variations in volume flux are not artifacts; at least not in the 285   model.

In Sect. 5.2, we argued that the hourly variations in volume flux were forced by sea level differences between the northern and southern ends of the estuary. From Fig. 7b, it appears that the same mechanism may be invoked for the 25-hour averaged flux. Periods with average southward flux have average sea levels higher north of the estuary than south of it and vice versa. Surprisingly, periods with northward volume flux (e.g., period 1) seem to require smaller sea level differences than periods 290   with southward flow (e.g., Period 2). Possibly, the explanation is to be found in the highly non-linear character of flow across the southern sill (Fig. 6) where the flux increases rapidly for small sea level differences.

With this interpretation, the problem is transferred to explaining why there are fortnightly variations in the 25-hour averaged sea level difference between both ends of the estuary. A priori, this might still be an artifact generated by the model, but Fig. 10 indicates that this is not the case. The similarity between Fig. 7b and Fig. 10 is not perfect. The observed signal in sea level 295   difference (Fig. 10b) is smaller than indicated by the model (Fig. 7b) and the lags are not identical. We should, however, not expect perfect similarity, because Tórshavn is rather far south of the southern end of the estuary (Fig. 1a).

When seeking explanations for these variations, the amphidromic character of the region is again an obvious candidate. Different semidiurnal constituents (e.g., M_2 and S_2) will have different characteristics of their amphidromic regions and the interaction between these may generate effects that vary fortnightly. Why this should generate low-frequency sea level varia- 300   tions with fortnightly time scales is not obvious and should be more thoroughly investigated.

An alternative explanation may be linked to the tidally rectified residual currrents that circulate the Faroes over the shelf (Larsen et al., 2008). These currrents vary in strength over the spring-neap cycle and would be expected to generate sea level slopes through geostrophy that should have a fortnightly variation. Conceivably, these variations may generate the fortnightly variations in sea level difference between both ends of our estuary that are needed to explain Fig. 7.

305   On the available evidence, none of these explanations can be validated more quantitatively. However, the effect is important, especially for fish farming activities, and may affect other Faroese sounds. A larger model domain and more comprehensive sea level and currrent observations would be beneficial to increase our knowledge. This is planned to be performed in a follow-up study, but will be too voluminous for this manuscript. Here, we note only that observations verify that there are fortnightly variations between sea level north of the estuary and south of it similar to those in the model. Possibly, the model exaggerates

310   the effect or shifts its timing, but the reality of the fortnightly variations seems well justified.

Since southward flow across the southern sill occurs during flood, it has been suggested that the cross-sectional area over the sill – and therefore also volume flux – should be higher during southward than northward flow, which would lead to a net southward volume flux varying between 50 and 175 m^3 s^{-1} in phase with the strength of the tidal amplitude (VandKvalitetsInstitutet, 1983). This is not supported by the model, which has a net flux that varies between northward and southward direction

315   on a fortnightly time scale (Fig. 7a). To check the effect suggested by (VandKvalitetsInstitutet, 1983), volume transport across the southern sill was calculated with and without varying sea level. On average, the difference was 14 m^3 s^{-1}. Thus, the effect is real, but much smaller than expected and swamped by the fortnightly variations.

5.4   Exchange rates/ flushing rates

For an estuary that is affected by human activity, one of the most important parameters is the flushing rate, i.e., how fast

320   the waters in the estuary (and dissolved contaminants or planktonic organisms) are flushed out of the estuary. An often used measure of this is the ***"flushing time"***, defined as the volume of the estuary (or parts of it) divided by the volume flux into or out of the estuary. Combining CTD observations from our estuary with estimated freshwater supply, Hansen (1990) estimated a typical flushing time of 5 days for this estuary, but noted the uncertainty for this value.

From the present model results, there are several ways of obtaining alternative estimates. One way is to use Fig. 5b, which

325   implies that between 5 and 10 % of the estuarine volume is typically flushed in and out over the northern sill every 12 hours. If one assumes no mixing between in-flowing and out-flowing waters, this method gives an average flushing time of around one week, ranging between less than four days and more than 11 days (Supplementary Fig. S7) over the simulation period.

Alternatively, one could use the average salinity distribution (Supplementary Fig. S3) to estimate the average total freshwater content in the estuary and combine that with the (almost constant) freshwater supply to calculate a flushing time. This method

330   is, however, very sensitive to the choice of seawater salinity that is diluted by freshwater and also assumes stationary conditions.

An extra challenge when trying to estimate a "typical" flushing time is the fortnightly variation in the net flow through the estuary (Sect. 5.3). Considering the two periods defined in Fig. 7, Figure 12 illustrates the two different exchange regimes, that the estuary regularly shifts between.
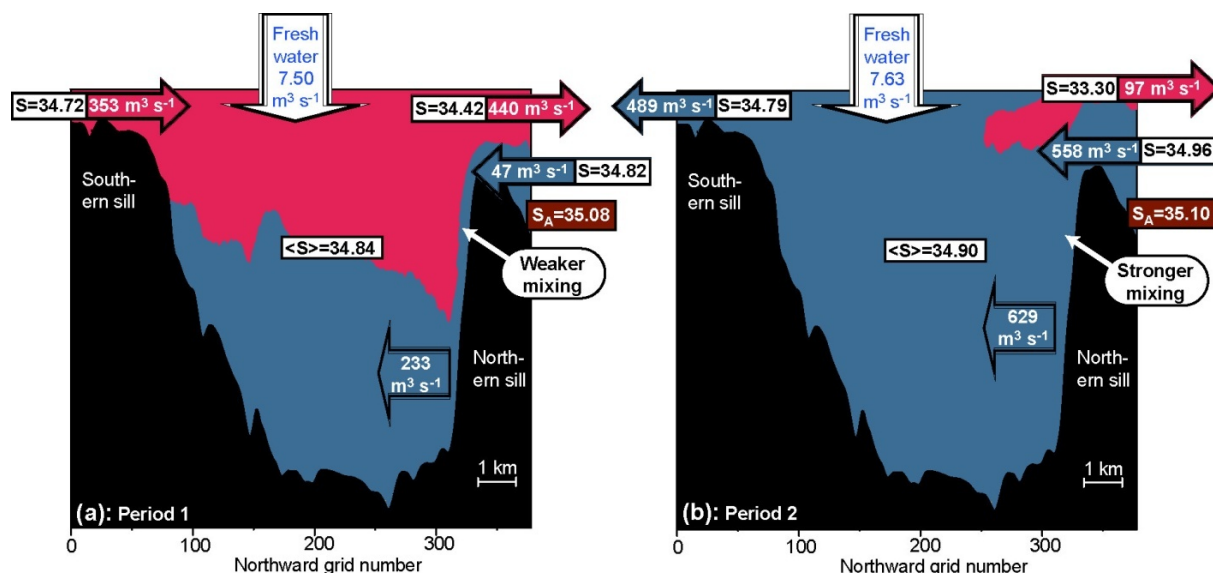
Figure 12. Schematic flow patterns and exchanges for the two periods defined in Fig. 7. Red and blue areas show north- and south-going (cross-estuary averaged) flow, respectively (based on Fig. 8). Horizontal arrows over the two sills show average volume flux and (flux-averaged) salinity over the sills for each period. The wide south-going arrow at depth for each period shows the total south-going volume flux just south of the northern sill (northward grid number 311). Vertical arrows show average freshwater supply to the estuary for each period, including river and hydropower supply (constant) as well as precipitation (variable). The values for $<S>$ are the salinities averaged over the whole estuary for each period. Brown boxes show the salinity, S_A, for the Atlantic water at depth north of the northern sill. Indications of mixing intensity over the slope south of the northern sill (white arrows) are based on Fig. 11.

The background colours in Fig. 12 indicate net (i.e., 25-hour average) flow through the estuary. The red areas in Fig. 12a

335 show that the upper layers have a net northward flow during Period 1. On an hourly time scale, water flows back and forth across the sills, but on average, there is a net flow from the region south of the southern sill, through the estuary, and out across the northern sill. The total volume of water carried through the estuary by this net flow during the 188 hours of Period 1 is slightly more than the volume of the estuary.

During Period 2, the net flow is quite different. Now, the blue colour in Fig. 12b indicates net southward flow through almost

340 the entire estuary. Only a small near-surface region close to the northern sill has net northward flow. Even though Period 2 (158 hours) is shorter than Period 1 (188 hours), the net amount of water flowing through the estuary is somewhat higher.

The most pronounced difference between the two periods lies in the net inflow from the north and its passage through the deep parts of the estuary. The net southward flow of seawater across the northern sill along the bottom was more than ten times higher during Period 2 (558 m^3 s^{-1}) than Period 1 (47 m^3 s^{-1}) and it was less diluted by the fresher waters on top. This is seen

345 by comparing the flux-averaged salinity of the southward inflow (values in arrows) with the salinity S_A of the more "pure" Atlantic water found at depth north of the estuary (values in brown boxes).

After passing over the northern sill, the dense seawater from the north tends to stay close to the bottom over the southern slope of the sill (Fig. 11d). This is the case during both periods, but more so during Period 1 (Fig. 8). During this descent, the seawater entrains and is diluted by water already in the estuary. Thus, the 47 m^3 s^{-1} that crossed the sill during Period 1 increased to 233 m^3 s^{-1} at depth (Fig. 12a).

During Period 2, the seawater from the north seems to experience stronger mixing with ambient waters (Fig. 11c) and to be more spread out through the water column (Fig. 8). The deep arrow in Fig. 12b showing 629 m^3 s^{-1} represents net southward flow through the whole water column just south of the northern sill, but most of that is below sill level of the northern sill. This is evident from Fig. 9, which also illustrates the difference in deep flow and flushing during the two periods.

If the arrows in Fig. 12 are combined to make budgets, we see that they do not balance. During both periods, Fig. 12 indicates more water leaving the estuary than entering it and the associated sea level changes would be unrealistically large. It has to be kept in mind, however, that the values in Fig. 12 are based on averages for each period with sea level kept constant. The volume flux estimates therefore have an uncertainty, which over the southern sill at least are on the order of 10 %. Within that uncertainty, there is balance. It might also be emphasized once again that the arrows in the figure are net volume fluxes, upon which are superimposed the semidiurnal variations with amplitudes that are considerably higher.

6 Recommendations

The fortnightly variations in net flow through our estuary revealed by the model may have large impacts on any development or activity that affects the estuary and its surroundings, such as hydropower development or fish farming. They should therefore be considered when planning future operations. We also recommend a more thorough validation of the model. Although the model results show a satisfactory agreement with the available observational data, these data were not targeted at some of the key processes that have appeared. We therefore recommend that a more targeted field experiment is implemented that can reveal more of the strengths and weaknesses of the model.

We also recommend investigating the mixing across the northern sill, to see if there is actually hydraulic jump conditions, with a model that is not using the hydrostatic assumption, thus beeing able to make conclusions on vertical advection.

375 *Author contributions.* SVE, JA and KS conceptualized the model study, JA set up the model and ran the model. SVE performed data analysis on model data, EO performed analysis on observations. KS, EK and BH provided supervision and guidance. SVE and BH wrote the manuscript with input from all the authors.

Competing interests. The authors declare that they have no conflict of interest.

References

Davidsen, E., Førland, E., and Madsen, H.: Orographically enhanced proecipitation on the Faroe Islands, in: Nordic Hydrological Conference
1994, edited by Kern-Hansen, C., Rosbjerg, D., and Thomsen, R., no. 34 in Nordic Hydrological Program (NHP) Report, pp. 229–239,
Nordic Association for Hydrology, Tórshavn, Faroe Islands, 1994.

Erenbjerg, S. V.: Avfall í Sundalagnum og hjáliggandi firðum, metingar og mátingar; Input til ROMS fresh water forcing, in: Fiskaaling rit,
Technical Report, 02, pp. 1–10, Fiskaaling P/F, Við Áir, Faroe Islands, 2020.

Erenbjerg, S. V., Albretsen, J., Simonsen, K., Sandvik, A. D., and Kaas, E.: A step towards high resolution modeling of the central Faroe shelf
circulation by FarCoast800, Regional Studies in Marine Science, 40, 101 475, https://doi.org/https://doi.org/10.1016/j.rsma.2020.101475,
2020.

Farmer, D. M. and Freeland, H. J.: The physical oceanography of Fjords, Progress in Oceanography, 12, 147–219,
https://doi.org/https://doi.org/10.1016/0079-6611(83)90004-6, 1983.

Haidvogel, D., Arango, H., Budgell, W., Cornuelle, B., Curchitser, E., Lorenzo, E., Fennel, K., Geyer, W., Hermann, A., Lanerolle, L.,
Levin, J., McWilliams, J., Miller, A., Moore, A., Powell, T., Shchepetkin, A., Sherwood, C., Signell, R., Warner, J., and Wilkin, J.:
Ocean forecasting in terrain-following coordinates: Formulation and skill assessment of the Regional Ocean Modeling System, Journal of
Computational Physics, 227, 3595–3624, https://doi.org/10.1016/j.jcp.2007.06.016, 2008.

Hansen, B.: Sea Level Variations and currents on the Faroe Plateau and their relation to the hydrography, Ph.D. thesis, University of Copen-
hagen, Institute of physical Oceanography/University of Faroe Islands, 1978.

Hansen, B.: Oxygentrot og útskifting í botnvatninum á føroyskum gáttarfirðum, Fiskirannsóknir, 6, 188–258, 1990.

Kragesteen, T. J., Simonsen, K., Visser, A. W., and Andersen, K. H.: Identifying salmon lice transmission characteristics between Faroese
salmon farms, Aquaculture Environment Interactions, 10, 49–, https://doi.org/10.3354/aei00252, 2018.

Larsen, K. M., Hansen, B., and Svendsen, H.: Faroe Shelf Water, Continental Shelf Research, 28, 1754–1768,
https://doi.org/10.1016/j.csr.2008.04.006, 2008.

Larsen, K. M. H., Mortensen, E., Øystein Patursson, and Simonsen, K.: Current measurements in the ASAF project, Deployment SUNB1212,
in: ASAF, no. 03 in Technical Report, pp. 1–22, Havstovan/Fiskaaling P/F, Tórshavn, Faroe Islands, 2014a.

Larsen, K. M. H., Mortensen, E., Øystein Patursson, and Simonsen, K.: Current measurements in the ASAF project, Deployment SUNC1212,
in: ASAF, no. 03 in Technical Report, pp. 1–22, Havstovan/Fiskaaling P/F, Tórshavn, Faroe Islands, 2014b.

Lien, V., Gusdal, Y., Albretsen, J., Melsom, A., and Vikebø, F.: Evaluation of a Nordic Seas 4 km numerical ocean model archive, Fisken og
Havet, 7, 7:79, 2013.

Myksvoll, M., Sandvik, A., Skarðhamar, J., and Sundby, S.: Importance of high resolution wind forcing on eddy activity and particle disper-
sion in a Norwegian fjord, Estuarine, Coastal and Shelf Science,, 113, 293–304, https://doi.org/https://doi.org/10.1016/j.ecss.2012.08.019,
2012.

Pyper, B. J. and Peterman, R. M.: Comparison of methods to account for autocorrelation in correlation analyses of fish data, Canadian Journal
of Fisheries and Aquatic Sciences, 55, 2127–2140, https://doi.org/10.1139/f98-104, 1998.

Rasmussen, T., Olsen, S. M., Hansen, B., Hátún, H., and Larsen, K. M.: The Faroe shelf circulation and its potential impact on the primary
production, Continental Shelf Research, 88, 171 – 184, https://doi.org/10.1016/j.csr.2014.07.014, 2014.

Shchepetkin, A. F. and McWilliams, J. C.: The regional oceanic modeling system (ROMS): A split-explicit, free-surface, topography-
following-coordinate oceanic model, Ocean Modelling, 9, 347 – 404, https://doi.org/10.1016/j.ocemod.2004.08.002, 2005.

Ocean Science
Discussions

EGU

420 Simonsen, K.: The Tides on the Faroe Shelf and an Attempt to Simulate the M_2-Tide in the Area, Master's thesis, Geophysical Institute, University of Bergen, 1992.

Simonsen, K. and Niclasen, B.: Analysis of the energy potential of tidal streams on the Faroe Shelf, Renewable Energy, 163, 834–844, https://doi.org/https://doi.org/10.1016/j.renene.2020.08.123, 2021.

Simonsen, K., Joensen, E., and Erenbjerg, S.: Sundalagið - Samandráttur av hydrografiskum mátingum árini 2013-2017, in: Fiskaaling rit,
425 Technical Report, 01, pp. 1–50, Fiskaaling P/F, Tórshavn, Faroe Islands, 2018.

VandKvalitetsInstitutet: Biologiske effekter af vandkraft ved Vestmanna og Eiði Færøerne, in: Rapport til Overfredningsnævnet på Færøerne, Technical Report, pp. 1–22, VKI, Tórshavn, Faroe Islands, 1983.